Pergamon

Int. J. Solids Structures Vol. 34, No. 30, pp. 4019–4035, 1997

0020-7683/97 $17.00 + .00

PII: S0020-7683(96)00234-X

TRANSIENT SCATTERING OF SH WAVES BY SURFACE-BREAKING AND SUB-SURFACE CRACKS

SHAW-WEN LIU
Department of Mathematics and Physics, Chinese Air Force Academy, P.O. Box 90277-4, Kangsan, Kaohsiung, Taiwan 82000, R.O.C.

and

JEN-CHUN SUNG and CHING-SEN CHANG
Department of Civil Engineering, National Cheng Kung University, Tainan, Taiwan 70101, R.O.C.

(*Received* 18 *July* 1995; *in revised form* 15 *November* 1996)

Abstract—The transient scattering of SH waves by surface-breaking and sub-surface cracks normal to the free surface of a half-space is investigated. The problem is first solved in the frequency domain by an efficient hybrid method which combines the finite element method (FEM) with the boundary integral representation (BIR). The transient responses are then obtained by inverting the spectra via fast Fourier transform (FFT) routine. The shape of the incident pulse is a Ricker wavelet. Graphical results are presented for the surface displacements, crack opening displacements, and dynamic stress intensity factors to show the significant effects due to the presence of the cracks. The wave propagation can be clearly observed, so that the mechanism of SH-wave scattering by cracks can be easily understood by this study. Furthermore, the scattered waves received on the free surface can be used successfully to detect the location, length, and depth of the crack. © 1997 Elsevier Science Ltd.

1. INTRODUCTION

Problems of scattering of elastic waves by a crack are of considerable importance in a variety of engineering applications. In ultrasonic nondestructive evaluation (NDE) techniques, the interest is in the scattered wave field which carries a great deal of information on the characteristics of the crack. In fracture mechanics, the interest is in the determination of the stress field near the crack-tip as a prerequisite to the study of crack propagation under dynamic loading. Among the crack configurations that are usually considered in NDE and fracture mechanics, the surface-breaking and sub-surface cracks are of distinct practical significance. One of the objectives of this paper is to enhance the theoretical understanding of the wave scattering mechanism by such cracks.

Scattering of elastic waves by a crack has been studied by many authors. Mendelsohn *et al.* (1980), Achenbach and Brind (1981a, 1981b), Brind and Achenbach (1981), and Keer *et al.* (1984) have used an integral equation approach to study scattering of elastic waves by surface-breaking and sub-surface cracks. Scattering of SH waves by surface-breaking cracks were studied by Stone *et al.* (1980) using an integral equation formulation and by Datta (1979) and Datta *et al.* (1982) using a matched asymptotic expansion technique valid at long wavelengths as well as a combined finite element and analytical expansion technique, which is useful for long and intermediate wavelengths. Kundu and Mal (1981) solved the inplane edge crack problem by the application of an asymptotic theory of diffraction. In all these studies attention was restricted to the response in frequency domain only. In recent years, Scandrett and Achenbach (1987), Saffari and Bond (1987), and Harumi and Uchida (1990) studied the time-domain responses of cracks by using a finite difference method. The transient response of the surface of a layered half-space with interface cracks, excited by a plane SH-wave, was investigated by Karim and Kundu (1988) using singular integral equations.

The method adopted here is a combined boundary integral and finite element approach. The finite element method is most suitable for modeling problems with complex geometries and different materials. Problems of multiple scattering by a cluster of scatterers or by scatterers embedded in a different material from the surrounding matrix can be dealt with as easily as the simpler problem of a single scatterer in a homogeneous material. The shape of the scatterer can be arbitrary. The boundary integral method automatically takes into account the radiation condition. Therefore, this hybrid method can utilize the versatility of the finite element method for detailed modeling in the near-field and the effectiveness of the boundary integral in the far-field. Recently, this method has been used by Liu *et al.* (1991) and Liu and Datta (1993) to study scattering of impact waves by cracks in a glass plate. Very good results have been obtained. Other similar hybrid methods which combine the analytical and the numerical approaches by dividing the geometry into near-field and far-field have been attempted by Dasgupta (1980), Murakami *et al.* (1981), Shah *et al.* (1982, 1986), Gupta *et al.* (1982), Eilouch and Sandhu (1986), Mita and Luco (1987), Mossessian and Dravinski (1987), Romanel and Kundu (1993), to name a few. In general, the advantages of one method are the disadvantages of the other, therefore a hybrid method is developed by taking advantage of the good features of each method while at the same time minimizing their undesirable features.

In this paper, the transient scattering of SH waves by surface-breaking and sub-surface cracks in a half-space is studied. The shape of the incident pulse is a Ricker wavelet (Ricker, 1977). Numerical results are presented for the surface displacements, crack opening displacements, and stress intensity factors as functions of frequency and time. SH waves are particularly attractive because of the simple nature of their interaction with cracks and other boundaries. Thus the movement of SH waves can be clearly observed and the mechanism of the SH-wave scattering by cracks can be easily understood. This study is an important step for the investigation on more complicated scattering problems.

2. PROBLEM DESCRIPTION

The geometry of the problem considered here is depicted in Fig. 1. A half-space containing a surface-breaking crack (or a sub-surface crack) of length d is subjected to a plane SH-wave with an angle of incidence θ. The problem geometry, material properties, and incident pulse are invariant in the y-direction. The problem has only a y-component of nonzero displacement, u_y, which is a function of x, z, and t. Thus the corresponding governing equation of motion is given by

$$\beta^2\left(\frac{\partial^2 u_y}{\partial x^2}+\frac{\partial^2 u_y}{\partial z^2}\right)=\frac{\partial^2 u_y}{\partial t^2}, \tag{1}$$

where β is the shear wave velocity. The surface of the half-space and the crack faces are

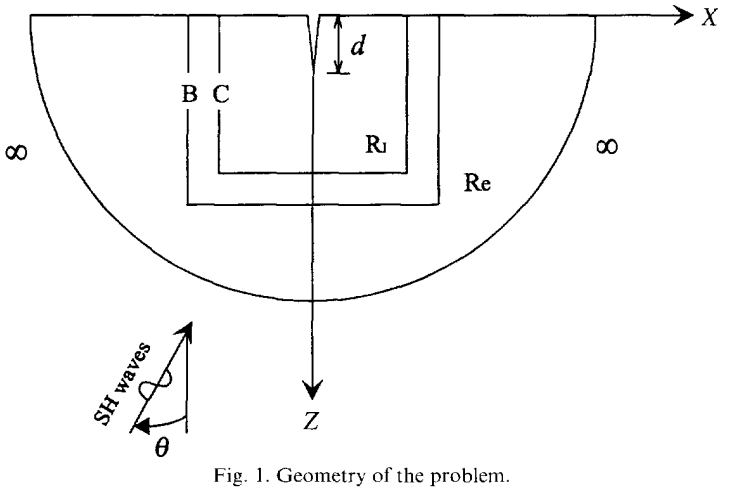

Fig. 1. Geometry of the problem.

assumed to be free of tractions. Usual radiation conditions should be satisfied by the scattered wave field at infinity.

3. FORMULATION

First the problem is solved in frequency domain, then the transient response is obtained by Fourier inversion of the spectrum. After Fourier transformation the governing equation in frequency domain takes the following form:

$$\beta^2\left(\frac{\partial^2 U}{\partial x^2}+\frac{\partial^2 U}{\partial z^2}\right)=-\omega^2 U, \tag{2}$$

where U is y-direction displacement in the Fourier transformed domain and ω is the circular frequency.

This problem is solved by a hybrid method which combines the finite element discretization of the vicinity of the crack with the boundary integral representation of the exterior scattered field. To solve the problem by this method, the crack should be completely enclosed by a fictitious contour C as shown in Fig. 1. In addition, two regions, R_i and R_e, are introduced here. The interior region, R_i, is bounded by a fictitious boundary B and discretized with finite elements. The exterior region, R_e, is bounded inside by the contour C. Based on the Betti's reciprocal theorem, an integral representation over C is used to solve for the exterior scattered field. The area between the contour C and boundary B is shared by both regions. The finite element analysis of the interior region is considered first.

3.1. *Finite element analysis for interior region*

The interior region, which encloses all the inhomogenities, is discretized into a set of finite elements. The finite element equations are derived in the frequency domain using a variational principle. In order to have a correct simulation for the stress field near the crack tips, six-node triangular quarter-point singular elements are used around the crack tips. The equation of motion for each element can be written in the following form:

$$\mathbf{K}_e\mathbf{d}_e-\omega^2\mathbf{M}_e\mathbf{d}_e=\mathbf{f}_e, \tag{3}$$

where $\mathbf{K}_e$ and $\mathbf{M}_e$ are the stiffness and mass matrices, respectively, $\mathbf{f}_e$ is the vector of nodal forces due to surface tractions, and $\mathbf{d}_e$ contains the nodal displacements of the element. Equation (3) can be written in a simple form:

$$\mathbf{S}_e\mathbf{d}_e=\mathbf{f}_e, \tag{4}$$

where the matrix $\mathbf{S}_e$ is the elemental impedance matrix and defined by

$$\mathbf{S}_e=\mathbf{K}_e-\omega^2\mathbf{M}_e. \tag{5}$$

The matrix $\mathbf{S}_e$ is computed for each element and assembled into global matrix $\mathbf{S}$. Therefore, the global equation of motion becomes

$$\mathbf{Sd}=\mathbf{f}. \tag{6}$$

Here, $\mathbf{d}$ and $\mathbf{f}$ represent all the nodal displacements and forces, respectively. The nodal displacement $\mathbf{d}_B$ at the boundary B can be separated from the interior nodal displacement $\mathbf{d}_I$. Partitioning of the matrices in eqn (6) results in the following equation

$$\begin{bmatrix} \mathbf{S}_{BB} & \mathbf{S}_{BI} \\ \mathbf{S}_{IB} & \mathbf{S}_{II} \end{bmatrix} \begin{Bmatrix} \mathbf{d}_B \\ \mathbf{d}_I \end{Bmatrix} = \begin{Bmatrix} \mathbf{f}_B \\ \mathbf{f}_I \end{Bmatrix}, \tag{7}$$

where $\mathbf{f}_B$ denotes the nodal force at the boundary B and $\mathbf{f}_I$ the interior nodal force. Since for problem considered here only the boundary B is subjected to surface tractions, there are no nodal forces on the interior nodes, i.e., $\mathbf{f}_I = 0$. Thus eqn (7) becomes

$$\begin{bmatrix} \mathbf{S}_{BB} & \mathbf{S}_{BI} \\ \mathbf{S}_{IB} & \mathbf{S}_{II} \end{bmatrix} \begin{Bmatrix} \mathbf{d}_B \\ \mathbf{d}_I \end{Bmatrix} = \begin{Bmatrix} \mathbf{f}_B \\ 0 \end{Bmatrix}. \tag{8}$$

This completes the analysis of the finite element formulation for the interior region. However, the nodal displacements $\mathbf{d}_B$ and $\mathbf{d}_I$ in eqn (8) can not be solved at this moment because the nodal force $\mathbf{f}_B$ is unknown. Thus, the formulation of the problem in the exterior region is considered next.

3.2. *Boundary integral representation for exterior region*

The exterior region is modeled by using a boundary integral representation. The total displacement field can be decomposed into two parts

$$U = U^S + U^F, \tag{9}$$

where the superscripts S and F denote the scattered and free fields, respectively. The free field can be obtained by solving the problem of the flawless half-space subjected to an incident SH-wave. The displacement solution of the free field is given by

$$U^F = 2A\cos(\eta z)e^{i\xi x}, \tag{10}$$

where $i = \sqrt{-1}$, $\eta = k_2\cos\theta$, $\xi = k_2\sin\theta$, k_2 is the wave number, and A is the amplitude of the incident wave. The scattered field is more complicated and can not be expressed by a simple form. Here, the displacement of the scattered field is represented by a line integral based on the Betti's reciprocal theorem as discussed below.

Let us consider two solution states I and II. Using Betti's reciprocal theorem these two states can be related in the following manner

$$\int_V (F_i^I U_i^{II} - F_i^{II} U_i^I)\,\mathrm{d}V = \int_S (T_i^{II} U_i^I - T_i^I U_i^I)\,\mathrm{d}S, \tag{11}$$

where F_i is the body force per unit volume and T_i is the surface traction per unit area. Subscript i indicates the ith direction. Superscripts I and II represent states I and II, respectively. For an antiplane problem all nonzero forces and displacements act in the y-direction. So for our problem the volume integral and the surface integral may be reduced to surface integral and line integral, respectively. Then the general eqn (11) takes the form:

$$\int_S (F^I U^{II} - F^{II} U^I)\,\mathrm{d}S = \int_L (T^{II} U^I - T^I U^{II})\,\mathrm{d}L. \tag{12}$$

In order to derive the boundary integral representation, first we need to solve the Green's elastodynamic state which corresponds to the problem of a flawless half-space subjected to a time harmonic line load at a source point (x_p, z_p). The equation of the Green's problem is given by

$$\beta^2\left(\frac{\partial^2 U^G}{\partial x^2}+\frac{\partial^2 U^G}{\partial z^2}\right)=-\omega^2 U^G-\frac{1}{\rho}\delta(x-x_p)\delta(z-z_p), \tag{13}$$

where the superscript G represents the Green's elastodynamic state, ρ is material density, and δ denotes the Dirac delta function. In addition, the Green's functions should satisfy stress-free boundary condition at the surface of the half-space and radiation condition at infinity. Then eqn (13) is solved to obtain the displacement of the Green's elastodynamic state

$$U^G=\frac{i}{4\pi\mu}\int_{-\infty}^{+\infty}\frac{1}{\nu_2}[e^{i\nu_2|z-z_p|}+e^{i\nu_2(z+z_p)}]e^{ik(x-x_p)}\,\mathrm{d}k, \tag{14}$$

where $\nu_2=\sqrt{k_2^2-k^2}$ and μ is the shear modulus. The corresponding stresses can be obtained by the constitutive relations. Finally, the boundary integral representation of the scattered field is derived next.

First, the Betti's reciprocal theorem, eqn (12), is applied to the region bounded by contour C. Two solution states considered here are the free field and the Green's field with its sources (x_p, z_p) on boundary B. Thus, the body forces for both fields are zero in this region. These two states can be related in the following manner

$$0=\int_C (T^G U^F-T^F U^G)\,\mathrm{d}C. \tag{15}$$

Secondly, the Betti's reciprocal theorem is applied to the exterior region. The scattered field is taken to be the first state and the Green's solution is the second state. The body force of scattered field is zero inside this region. Reversing the direction of integration, eqn (12) becomes

$$U^S(x_p, z_p)=\int_C (T^G U^S-T^S U^G)\,\mathrm{d}C. \tag{16}$$

Therefore, both eqn (15) and eqn (16) have the same direction of integration. They can be added together to form the boundary integral representation of the scattered field

$$U^S(x_p, z_p)=\int_C (T^G U-T U^G)\,\mathrm{d}C. \tag{17}$$

The boundary integral representation of the total displacements at the nodal points on boundary B is then obtained by using eqn (9)

$$U(x_p, z_p)=\int_C (T^G U-T U^G)\,\mathrm{d}C+U^F. \tag{18}$$

3.3. *Combination of FEM and BIR*

The integral in eqn (18) can be discretized by using the finite element formulation. Then eqn (18) becomes

$$\mathbf{d}_B=\mathbf{A}_{BB}\mathbf{d}_B+\mathbf{A}_{BI}\mathbf{d}_I+\mathbf{d}_B^F \tag{19}$$

where $\mathbf{A}_{BB}$ and $\mathbf{A}_{BI}$ are complex matrices and $\mathbf{d}_B^F$ is the free field displacement at nodal points on boundary B. Now combining eqn (19) with the second equation of eqn (8), we obtain

$$\begin{bmatrix} \mathbf{I}-\mathbf{A}_{BB} & -\mathbf{A}_{BI} \\ \mathbf{S}_{IB} & \mathbf{S}_{II} \end{bmatrix} \begin{Bmatrix} \mathbf{d}_B \\ \mathbf{d}_I \end{Bmatrix} = \begin{Bmatrix} \mathbf{d}_B^F \\ 0 \end{Bmatrix}. \tag{20}$$

Equation (20) is usually a large sparse unsymmetric complex matrix equation. For a transient problem the finite element meshes should be fine enough to capture the characteristics of wave at the highest frequency. This increases the degrees of freedom of the problem. Thus some numerical techniques are needed to reduce both computation time and required storage. A compacted data structure (Nour-Omid and Taylor, 1984) is adopted to store only the non-zero terms of the sparse matrix in a vector form, then the biconjugate gradient method (Sarkar *et al.*, 1981 and Sarkar, 1987) is used to solve eqn (20). The biconjugate gradient method, which is an iterative method, involves only the multiplication of matrix and vector, therefore the sparsity pattern of the matrix is not destroyed. For the scattering problem considered here, these numerical techniques are very efficient and always provide a satisfactory solution.

Once the nodal displacements ($\mathbf{d}_B$ and $\mathbf{d}_I$) are solved from eqn (20), the displacements in the interior region and in the exterior region can be easily computed by using finite element method and boundary integral representation, respectively. The transient response is then obtained by Fourier inversion of the spectrum.

3.4. *Crack opening displacements and stress intensity factors*

The crack opening displacements C_y is obtained by the displacements along the crack faces. For a vertical crack considered here, the crack opening displacement is given by the following form

$$C_y = U(0^+, z) - U(0^-, z). \tag{21}$$

Around the crack tip six-node triangular quarter-point elements (Barsoum, 1977) are chosen to obtain the correct square root singularity near the tip. The stress intensity factor K_{III} can be calculated from the crack opening displacements near the crack tip. The formula for computing the stress intensity factor was given by Datta and Shah (1982) as the following form:

$$K_{III} = \frac{\mu}{2\sqrt{2L}}[4(U_6 - U_4) - (U_3 - U_2)], \tag{22}$$

where L is the length of the singular element along the crack faces and U_i is the displacement at node i as defined in Fig. 2.

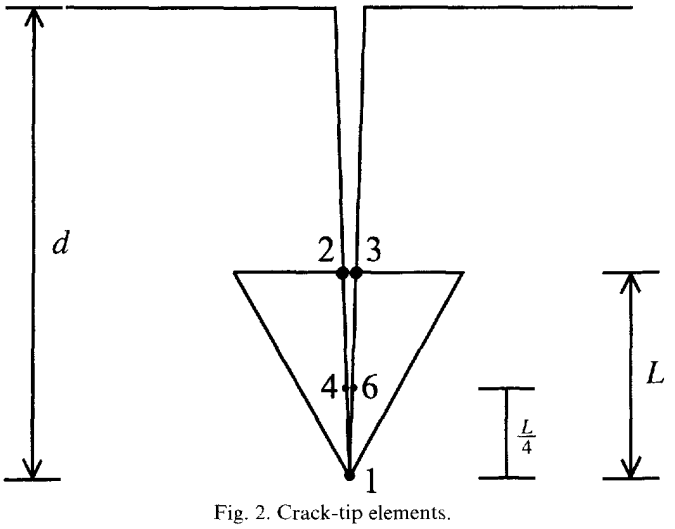

Fig. 2. Crack-tip elements.

4. NUMERICAL MODELING AND ACCURACY

In this study two vertical cracks of length d are considered. One is a surface-breaking crack and the other is a sub-surface crack which is deeper than the surface-breaking crack by $d/4$. The variables used here are presented in nondimensional form. The spatial coordinates are normalized with respect to the length of the crack. The nondimensional frequency ($\bar{f}$) and nondimensional time ($\bar{t}$) are defined as

$$\bar{f} = \frac{fd}{\beta} \tag{23}$$

and

$$\bar{t} = \frac{t\beta}{d}, \tag{24}$$

respectively. The calculated responses are normalized relative to amplitude of the incident wave. The normalized shear wave velocity is equal to 1.0.

In order to have an accurate simulation and a better visualization for the phenomena of transient wave scattering, a careful modeling is necessary. In general, the characteristic wavelengths of the incident pulse must be of the same order of magnitude as the characteristic dimension of the flaw, such as the crack length. On the other hand, the maximum frequency and the number of sample points must be determined so that not only the characteristics of the transient scattering can be captured but also the numerical accuracy and computational cost can be optimized. In this study, $\bar{f} = 4.0$ is chosen as the maximum frequency and 64 sample points are used for the numerical modeling. The incident pulse is a Ricker wavelet defined as

$$u(t) = (2\pi^2 f_c^2 t^2 - 1)\exp(-\pi^2 f_c^2 t^2) \tag{25}$$

where f_c is the characteristic frequency of the pulse. The Fourier transform of the Ricker wavelet is

$$U(f) = -\frac{2f^2}{\sqrt{\pi} f_c^3}\exp\left(-\frac{f^2}{f_c^2}\right), \tag{26}$$

which has a peak amplitude at $f = f_c$. Figure 3a shows the shape of the Ricker pulse with characteristic frequency $\bar{f}_c = 1.0$ and the corresponding spectrum is shown in Fig. 3b. In this paper, only $\bar{f}_c = 1.0$ are considered, in which the wavelength of the shear wave is equal to the crack length d.

Once the maximum frequency is determined, the size of the largest finite element can be chosen according to the desired numerical accuracy. Generally, 10 nodes per wavelength are adequate to accomplish the accuracy desired.

To verify the numerical accuracy, the zero-scattering test was checked first to keep the relative error of the computed total displacement and the incident field displacement within 5%. We also tested the accuracy by comparing the results obtained by the hybrid method used here with other available solutions. Figures 4 and 5 show the crack opening displacements at three different frequencies ($k_2 d = 1.0$, 4.7, and 15.7) and the stress intensity factors ($0 \leqslant k_2 d \leqslant 20$), respectively, for a surface-breaking crack in comparison with those presented by Stone *et al.* (1980). The angle of incidence is $\theta = 45°$. Agreement is found to be quite good. Then the detailed numerical results are studied in the next section.

5. RESULTS AND DISCUSSIONS

The surface displacements, crack opening displacements, and stress intensity factors are presented in both frequency and time domains for incident angle $\theta = 30°$. For the

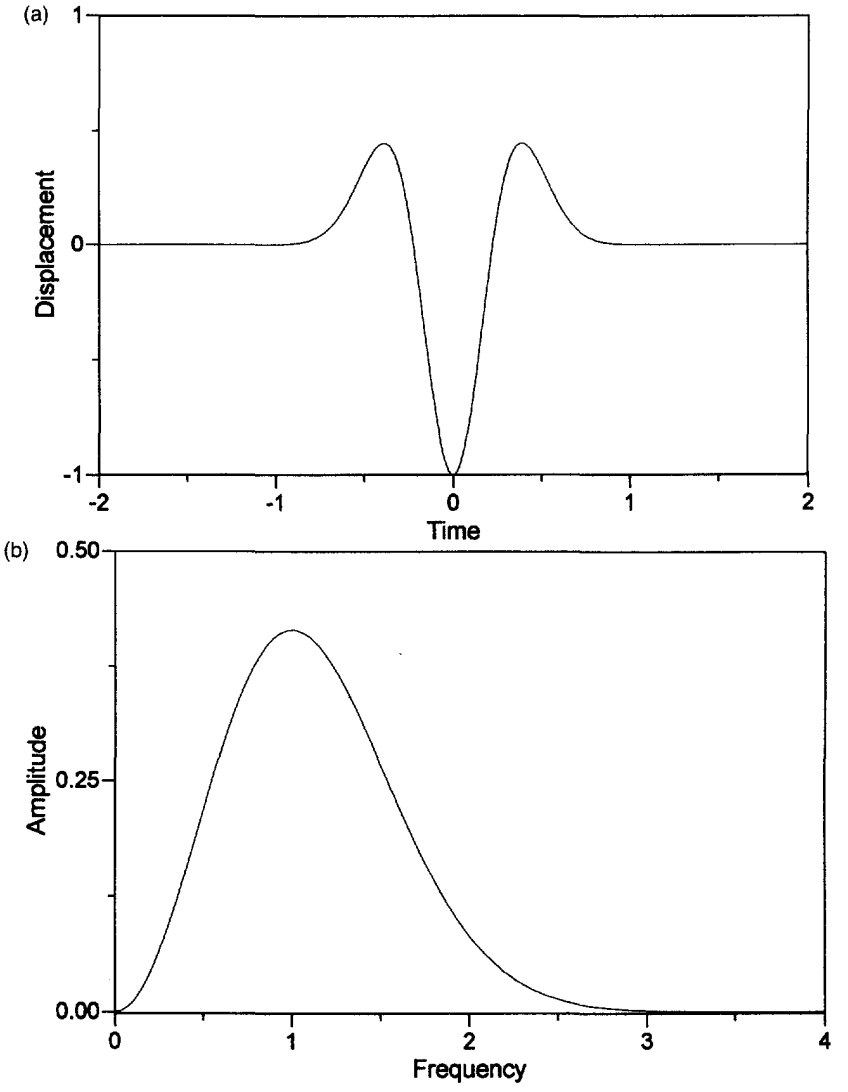

Fig. 3. (a) The shape of Ricker pulse and (b) the corresponding spectrum with characteristic frequency $\bar{f}_c = 1.0$.

responses in frequency domain, only the spectra caused by the delta pulse are presented. Because the frequency responses corresponding to any other incident pulses, such as a Ricker pulse, can be easily obtained by multiplying these spectra by the spectrum of the incident pulse itself. Note that in order to have a better visualization for the wave propagation the time when the peak value of Ricker pulse arrives at the origin ($x = z = 0$) has been set to $\bar{t} = 3.2$ for all the figures showing the transient responses in this paper.

5.1. *Surface-breaking crack*

Figure 6 illustrates the interaction between a plane SH-wave propagating at an incident angle θ and a surface-breaking crack in a half-space. This figure may be helpful to understand the following numerical results which contain the mechanism of reflection and diffraction occurred around a crack.

Displacement responses in frequency and time domains at 70 different points on the free surface from $x/d = -2.0$ to 2.0 are shown in Figs 7a and 7b, respectively. Due to the reflection from the left crack-face, larger amplitudes are observed in both figures in the region $x \leqslant 0$ close to the crack mouth. The response spectra become more complicated at higher frequencies because the scattering is more sensitive to short wavelength. Note that two thicker curves in Fig. 7b indicate the responses at the crack mouth. The responses in

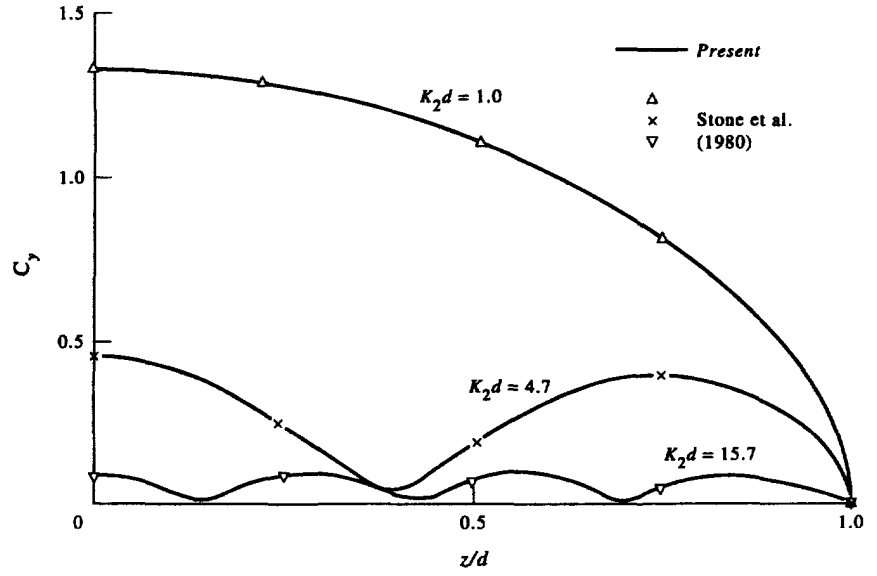

Fig. 4. Comparison of crack opening displacements of a surface-breaking crack in a half-space subjected to incident SH-waves with incident angle $\theta = 45°$.

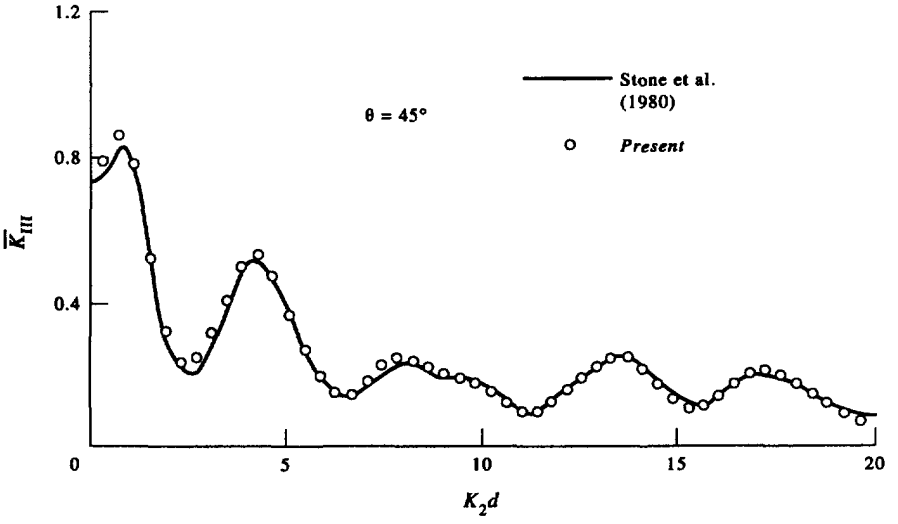

Fig. 5. Comparison of stress intensity factors of a surface-breaking crack in a half-space subjected to incident SH-waves with incident angle $\theta = 45°$.

the region $(-1/8 \leqslant x/d \leqslant 1/8)$ which has dense observation points are obtained by finite element method. Beyond that region, the results are calculated from boundary integral representation.

From Fig. 7b it is observed that the plane SH pulse with incident angle $\theta = 30°$ arrives at the crack mouth when $\bar{t} = 3.2$ and causes larger amplitudes on the left side of crack mouth. Then two scattered waves diffracted from the crack-tip appear anti-symmetrically on the free surface during $\bar{t} \approx 3.3 \sim 4.6$ and $\bar{t} \approx 5.1 \sim 6.3$, respectively. The first one originates from the diffraction of direct incident waves by the crack-tip at $\bar{t} \approx 2.3$. Note that part of first scattered waves are mixed with incident waves because their arrival times are very close. The second one is caused by the diffraction occurred at $\bar{t} \approx 4.1$ when the reflected waves from the free surface interact with crack-tip. In general, the scattered wave field contains a great deal of information about the characteristics of the crack. As shown in Fig. 7b, the crack can be easily located by the scattered waves observed on the free surface. Based on the transit times for scattered waves following various paths around the crack, the depth of crack-tip can be estimated by the following equation,

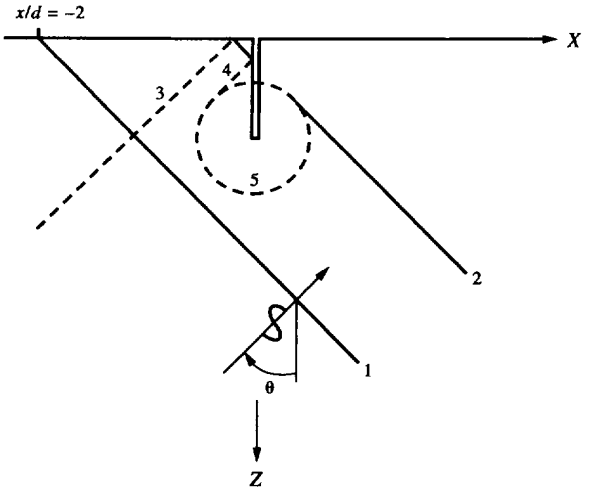

Fig. 6. Diffraction of a plane SH-wave by a surface-breaking crack in a half-space. 1,2 = incident waves; 3 = reflected wave from the free surface of half-space; 4 = reflected wave from crack face; 5 = diffracted wave from crack-tip.

$$d = \frac{1}{2\beta\Delta t}\sqrt{[x_2^2-(x_1+\beta\Delta t)^2][x_2^2-(x_1-\beta\Delta t)^2]}, \tag{27}$$

where Δt is the time difference for scattered waves arriving at $x = x_1$ and x_2 on the free surface.

Figure 8a shows the response spectra of crack opening displacements (COD) at the crack mouth and in the middle of crack. It is found that the amplitudes of COD at the crack mouth are usually larger than those in the middle of crack and the number of peak amplitudes at the crack mouth is about twice as many as that in the middle of crack. It is important to notice that the regular appearance of peaks in Fig. 8a at some specific frequencies can provide useful indication for the geometry of the crack. The frequency at which the resonance peak occurs is called the resonance frequency which is closely related to the crack length. For the resonance frequencies of the two-dimensional scattering problems, no closed form solutions are available. However, for a similar one-dimensional model, the resonance frequencies $\bar{f}_r$ can be expressed as

$$\bar{f}_r = \frac{f_r d}{\beta} = \frac{1}{4}(2n+1), \quad n = 0, 1, 2, \ldots \tag{28}$$

It is interesting to see that the resonance frequencies shown in Fig. 8a are close to the values calculated from eqn (28). Thus, the one-dimensional model may be a good approximation for the problem considered here.

Figure 8b shows the transient crack opening displacements along the whole crack length from $z/d = 0$ to 1. From Figs 8b and 6, the wave propagation and scattering around a surface-breaking crack can be understood thoroughly. The incident pulse arrives at the crack-tip when $\bar{t} \approx 2.3$ and a diffracted wave is created by the crack-tip at the same time. Then the incident wave and the diffracted wave reach the crack mouth at $\bar{t} \approx 3.2$ and 3.3, respectively. Therefore very large amplitudes are observed near the crack mouth. The reflected wave from the free surface ($x \leqslant 0$) strikes the left crack face from $\bar{t} \approx 3.2$ to 4.1. This causes very large CODs along the whole crack length. The reflected wave is then diffracted by the crack-tip as soon as it travels to the crack-tip at $\bar{t} \approx 4.1$. It is observed clearly in Fig. 8b that this diffracted wave propagates back and forth along the crack and its amplitude is dispersed gradually. Comparing Figs 8b and 7b, the phenomena of wave scattering around the crack are consistent with the responses observed on the free surface.

The response spectrum and the time history of stress intensity factor are shown in Figs 9a and 9b, respectively. Since the stress intensity factor is related to the COD, it is found

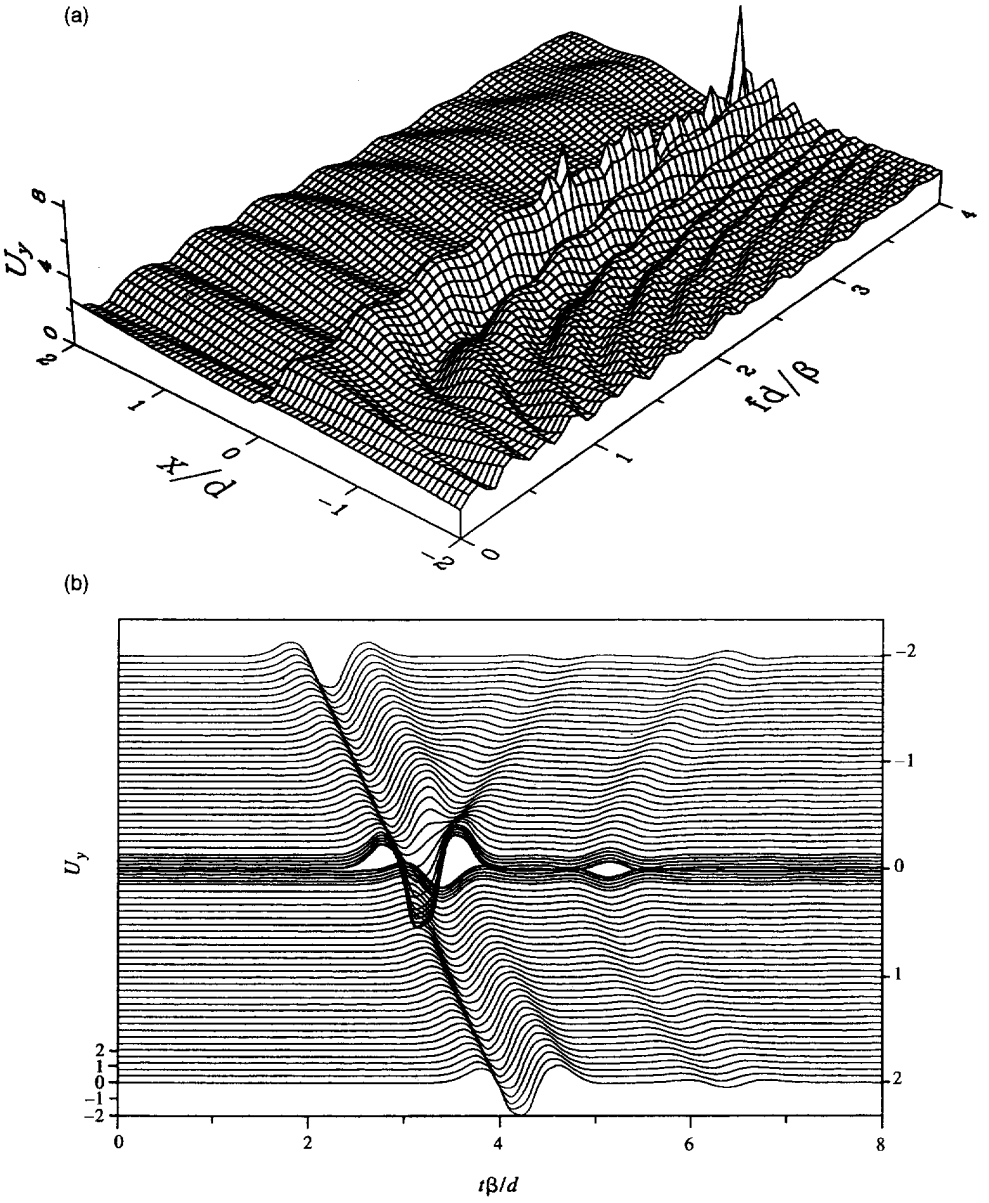

Fig. 7. Surface displacements for the case of surface-breaking crack: (a) response spectra and (b) time histories on the free surface from $x/d = -2.0$ to 2.0.

that the response spectra of $\bar{K}_{III}$ shown in Fig. 9a and COD at the crack mouth shown in Fig. 8a have similar patterns. In Fig. 9b, a pulse appears at $\bar{t} \approx 2.3$ because the direct incident wave arrives at crack-tip at that time. At time around $\bar{t} \approx 4.1$, very large amplitudes are produced due to the arrivals of reflected waves of incident and first diffracted waves from the free surface. Finally, the appearance of a small pulse at $\bar{t} \approx 6.1$ is caused by the arrival of reflected wave of second diffracted wave from the free surface. As was expected, the result of $\bar{K}_{III}$ shown here coincides with the result of near-tip COD shown in Fig. 8b.

5.2. *Sub-surface crack*

After a detailed study of the surface-breaking crack in the last sub-section, the case of sub-surface crack becomes much easier. Figures 10a and 10b show the response spectra and the time histories of the displacements on the free surface, respectively. Due to the existence of two tips for the sub-surface crack, it is expected that more diffracted waves will be created by tips. The incident wave is first diffracted by the lower tip at $\bar{t} \approx 2.1$ and its diffracted wave arrives at $x/d = 0 \sim \pm 2.0$ on the free surface during $\bar{t} \approx 3.4 \sim 4.5$. Then

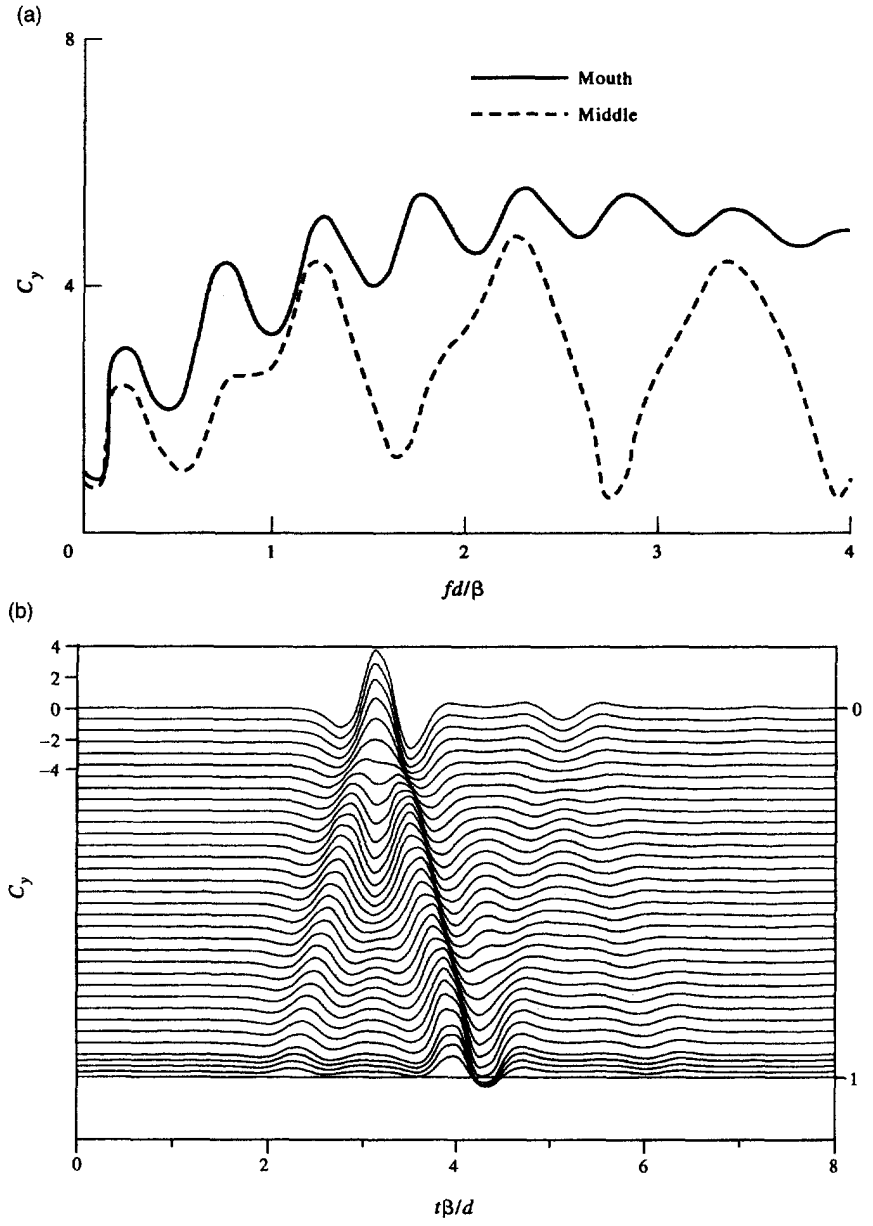

Fig. 8. Crack opening displacements for the surface-breaking crack: (a) response spectra at crack mouth and in the middle of crack and (b) time histories along the whole crack length.

the incident wave is diffracted by the upper tip at $\bar{t} \approx 3.0$. It is observed in Fig. 10b that this diffracted wave causes striking responses on the free surface during $\bar{t} \approx 3.2 \sim 5.0$. Similarly, the reflected wave from the free surface is diffracted by the upper and lower tips at $\bar{t} \approx 3.3$ and 4.3 and their diffracted waves travel to $x/d = 0 \sim \pm 2.0$ during $\bar{t} \approx 3.7 \sim 5.4$ and $5.5 \sim 6.6$, respectively. It is found that the diffracted wave caused by lower tip can be easily distinguished from the other diffracted waves. All of the diffracted waves can be used to find the location of crack. Furthermore, the depth of crack tips and crack length can be estimated by making use of eqn (27).

Figure 11a shows the response spectrum of COD in the middle of the sub-surface crack. It is observed that a series of distinct peaks and vales appears by turns in the response spectrum. Comparing with a similar and simple one-dimensional vibration problem in which both crack-tips are considered to be nodes in the normal modes, the peaks and vales seem to correspond to the antinodes and nodes. Similarly, the response spectra of stress intensity factors shown in Fig. 12a also appear as a series of regular peaks for both upper

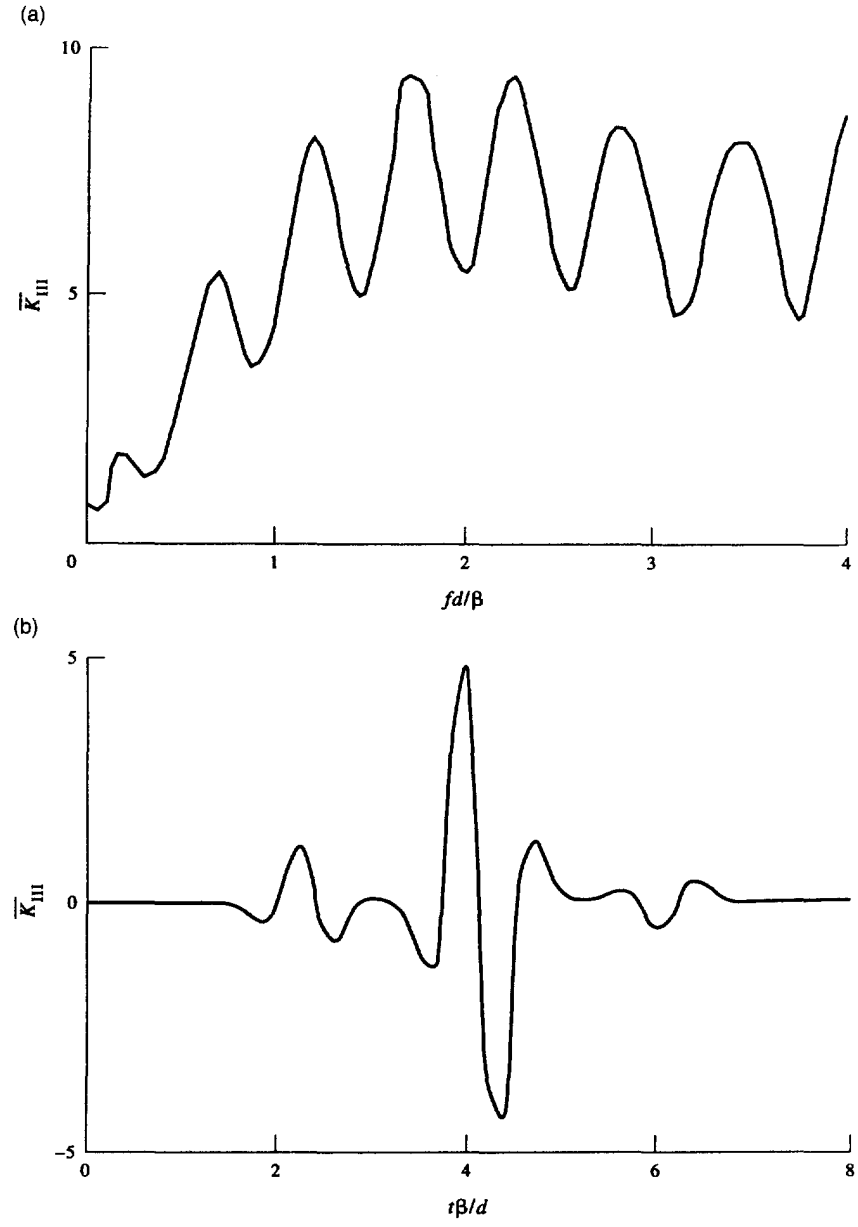

Fig. 9. Stress intensity factors for the surface-breaking crack: (a) response spectrum and (b) time history.

and lower tips. The frequencies corresponding to these peaks and vales are the resonance frequencies which are closely related to the crack length. However, an exact relationship between resonance frequencies and crack length is not available. In fact, the resonance frequencies are not only related to the crack length but also related to the distance between the free surface and the upper tip, boundary conditions of the system, material properties, and incident wave type.

Figure 11b shows the time histories of COD along the whole crack length from $z/d = 0.25$ to 1.25. It is found that the pattern of COD response here is analogous to that of surface-breaking crack shown in Fig. 8b. The incident SH-pulse travels to the lower and upper tips at $\bar{t} \approx 2.1$ and 3.0, respectively. It is seen during this period that the amplitudes of CODs become larger from lower tip to upper tip. Thus we may expect that stress intensity factor for upper tip at $\bar{t} \approx 3.0$ has higher value than that for lower tip at $\bar{t} \approx 2.1$. This is exactly what we observe in Fig. 12b which shows the transient stress intensity factors for

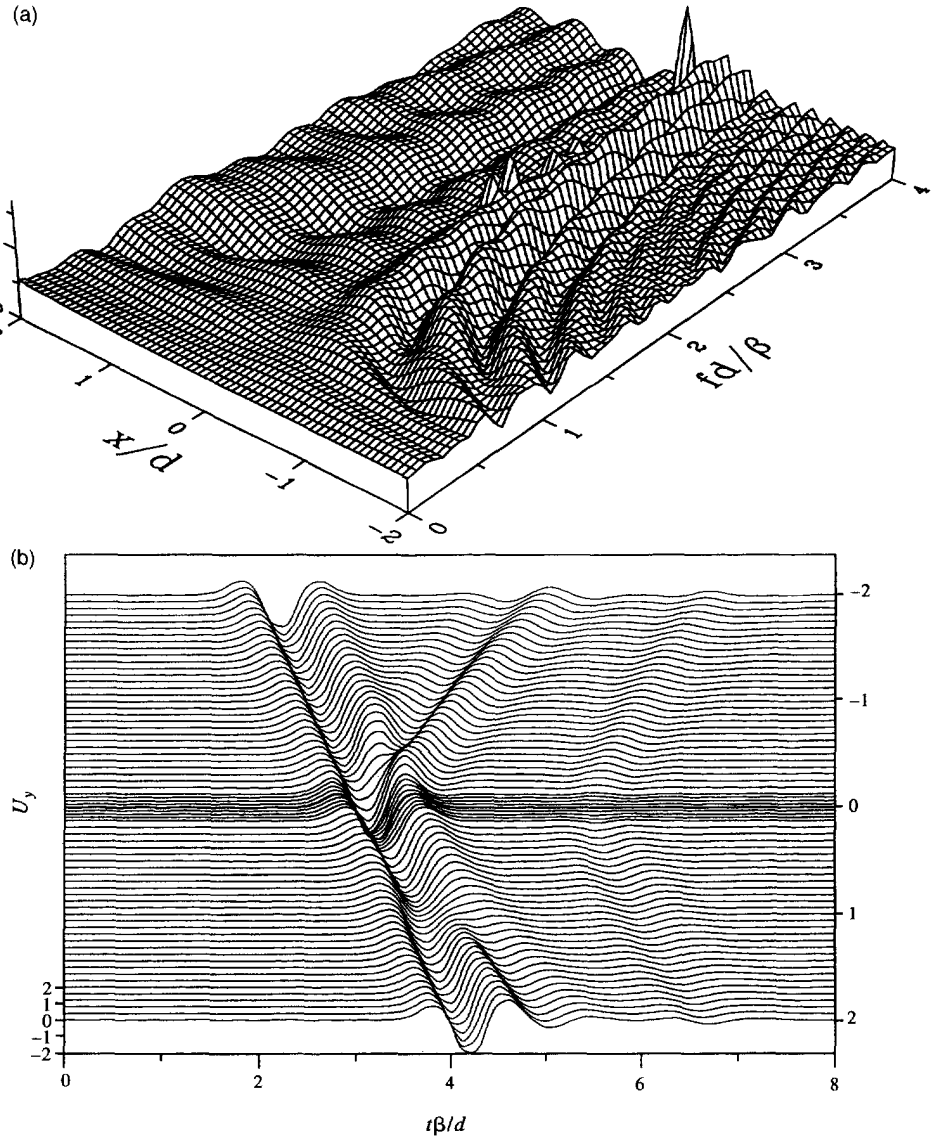

Fig. 10. Surface displacements for the case of sub-surface crack: (a) response spectra and (b) time histories on the free surface from $x/d = -2.0$ to 2.0.

both tips. In a little while, the reflected wave from the free surface arrives at upper and lower tips at $\bar{t} \approx 3.4$ and 4.3, respectively. Similarly, the effects of the reflected wave on the CODs and stress intensity factors can be clearly observed in Figs 11b and 12b. Note that the lower tip has the largest value of stress intensity factor around $\bar{t} \approx 4.3$ while the reflected wave arrives. Compared to the incident and reflected waves, the diffracted waves are smaller so that the effects of diffracted waves are not obvious during the period $\bar{t} \approx 2.1$ to 4.3. However, after the incident and reflected waves propagate away from the crack, the effects of diffracted wave caused by the interaction between reflected wave and lower tip at $\bar{t} \approx 4.3$ are very striking as shown in Figs 11b and 12b. It is seen obviously that this diffracted wave reaches the upper tip at $\bar{t} \approx 5.3$. Although the diffracted waves become smaller after $\bar{t} \approx 5.3$, the effects of diffracted waves can still be observed.

6. CONCLUSIONS

The scattering of SH waves by a surface-breaking and a sub-surface cracks has been investigated numerically by a hybrid method which combines the finite element method with the boundary integral representation. A detailed study on the surface displacements,

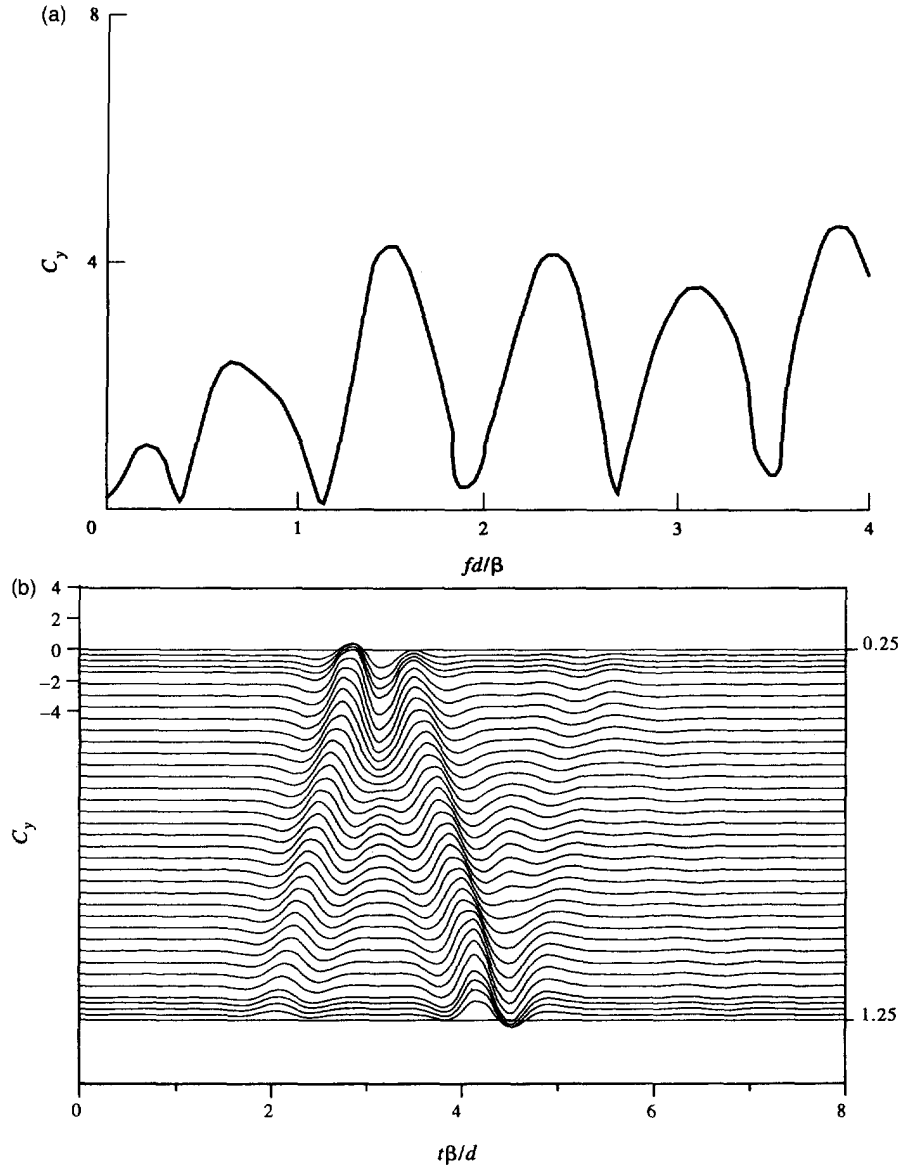

Fig. 11. Crack opening displacements for the sub-surface crack : (a) response spectrum in the middle of crack and (b) time histories along the whole crack length.

crack opening displacements, and dynamic stress intensity factors gives the following concluding remarks:

1. Due to the simple nature of SH-wave, the movement of individual diffracted wave or reflected wave can be easily identified and clearly observed. Hence the mechanism of SH-wave scattering by cracks can be understood thoroughly. This study is an important step for the further investigation on more complicated scattering problems, such as inplane problems.
2. Numerical results show that the location, length, and depth of the crack can be successfully detected and measured by the surface responses. This study is interesting in the viewpoint of quantitative nondestructive evaluation (QNDE).
3. The hybrid method adopted here is a very efficient method and suitable modeling for solving the forward problems. To solve an inverse problem, a large number of corresponding forward problems need to be solved. Therefore this hybrid method may be available for inverse problems.

Acknowledgements—This research was supported by the National Science Council, Republic of China under Contract Number NSC 82-0410-E-006-325.

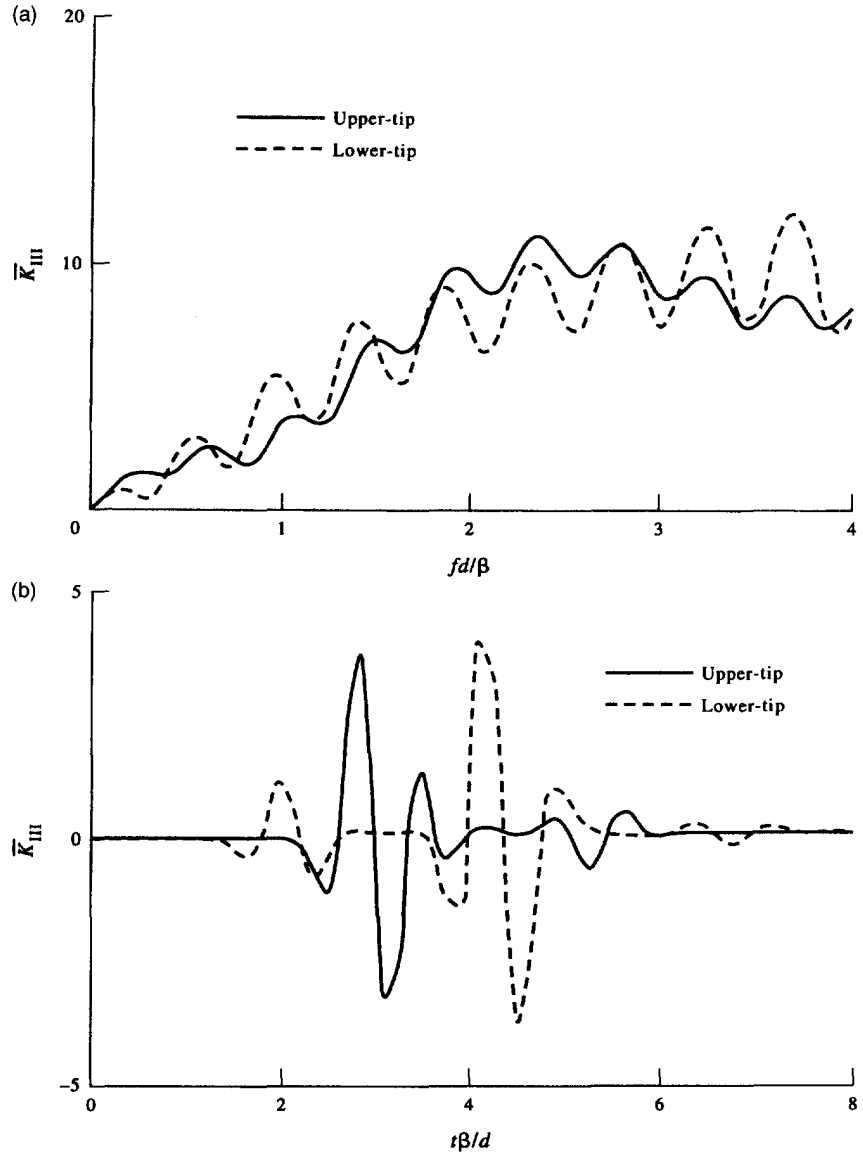

Fig. 12. Stress intensity factors for the sub-surface crack : (a) response spectra and (b) time histories.

REFERENCES

Achenbach, J. D., Keer, L. M. and Mendelsohn, D. A. (1980) Elastodynamic analysis of an edge crack. *Journal of Applied Mechanics* **47,** 551–556.

Achenbach, J. D. and Brind, R. J. (1981a) Elastodynamic stress-intensity factors for a crack near a free surface. *Journal of Applied Mechanics* **48,** 539–542.

Achenbach, J. D. and Brind, R. J. (1981b) Scattering of surface waves by a sub-surface crack. *Journal of Sound and Vibration* **76,** 43–56.

Barsoum, R. S. (1977) Triangular quarter-point elements as elastic and perfectly plastic crack tip elements. *International Journal of Numerical Methods in Engineering* **11,** 85–98.

Brind, R. J. and Achenbach, J. D. (1981) Scattering of longitudinal and transverse waves by a sub-surface crack. *Journal of Sound and Vibration* **78,** 555–563.

Datta, S. K. (1979) Diffraction of SH-waves by an edge crack. *Journal of Applied Mechanics* **46,** 101–106.

Datta, S. K., Shah, A. H., and Fortunko, C. M. (1982) Diffraction of medium and long wavelength horizontally polarized shear waves by edge cracks. *Journal of Applied Physics* **53,** 2895–2903.

Datta, S. K. and Shah, A. H. (1982) Scattering of SH waves by embedded cavities. *Wave Motion* **4,** 265–283.

Dasgupta, G. (1980) Foundation impedance matrices by substructure deletion. *Journal of the Engineering Mechanics Division ASCE* **106,** 517–523.

Eilouch, M. N. A. and Sandhu, R. S. (1986) A mixed method for transient analysis of soil-structure interaction under SH-motion. *Earthquake Engineering and Structural Dynamics* **14,** 499–516.

Gupta, S., Penzien, J., Lin, T. W. and Yeh, C. S. (1982) Three-dimensional hybrid modelling of soil-structure interaction. *Earthquake Engineering and Structural Dynamics* **10,** 69–87.

Harumi, K. and Uchida, M. (1990) Computer simulation of ultrasonics and its applications. *Journal of Non-destructive Evaluation* **9,** 81–99.

Karim, M. R. and Kundu, T. (1988) Transient surface response of layered isotropic and anisotropic half-spaces with interface cracks: SH case. *International Journal of Fracture* **37,** 245–262.

Keer, L. M., Lin, W. and Achenbach, J. D. (1984) Resonance effects for a crack near a free surface. *Journal of Applied Mechanics* **51,** 65–70.

Kundu, T. and Mal, A. K. (1981) Diffraction of elastic waves by a surface crack on a plate. *Journal of Applied Mechanics* **48,** 570–576.

Liu, S. W., Datta, S. K. and Ju, T. H. (1991) Transient scattering of Rayleigh-Lamb waves by a surface-breaking crack: comparison of numerical simulation and experiment. *Journal of Nondestructive Evaluation* **10,** 111–126.

Liu, S. W. and Datta, S. K. (1993) Scattering of ultrasonic wave by cracks in a plate. *Journal of Applied Mechanics* **60,** 352–357.

Mendelsohn, D. A., Achenbach, J. D. and Keer, L. M. (1980) Scattering of elastic waves by a surface-breaking crack. *Wave Motion* **2,** 277–292.

Mita, A. and Luco, J. E. (1987) Dynamic responses of embedded foundations: a hybrid approach. *Computer Methods in Applied Mechanical Engineering* **63,** 233–259.

Mossessian, T. K. and Dravinski, M. (1987) Application of a hybrid method for scattering of P, SV, and Rayleigh waves by near-surface irregularities. *Bulletin of the Seismic Society of America* **77,** 1784–1803.

Murakami, H., Shioya, S., Yamada, R. and Luco, J. E. (1981) Transmitting boundaries for time-harmonic elastodynamics of infinite domains. *International Journal of Numerical methods in Engineering* **17,** 1697–1716.

Nour-Omid, B. and Taylor, R. L. (1984) An algorithm for assembly of the stiffness matrices into a compacted data structure. *Engineering Computing* **1,** 312–316.

Ricker, N. H. (1977) *Transient waves in visco-elastic media.* Elsevier, Amsterdam, Holland.

Romanel, C. and Kundu, T. (1993) A hybrid modelling of soil-structure interaction problems for deeply embedded structures in a multilayered medium. *Earthquake Engineering and Structural Dynamics* **22,** 557–571.

Saffari, N. and Bond, L. J. (1987) Body to Rayleigh wave mode-conversion at steps and slots. *Journal of Nondestructive Evaluation* **6,** 1–22.

Sarkar, T. K., Siarkiewicz, K. and Stratton, R. (1981) Survey of numerical methods for solution of large systems of linear equations for electromagnetic field problems. *IEEE Transcriptions of Antennas Propagation* **29,** 847–856.

Sarkar, T. K. (1987) On the application of the generalized biconjugate gradient method. *Journal of Electromagnetic Waves and Applications* **1,** 223–242.

Scandrett, C. L. and Achenbach, J. D. (1987) Time-domain finite difference calculations for interaction of an ultrasonic wave with a surface-breaking crack. *Wave Motion* **9,** 171–190.

Shah, A. H., Wong, K. C. and Datta, S. K. (1982) Diffraction of plane SH waves in a half-space. *Earthquake Engineering and Structural Dynamics* **10,** 519–529.

Shah, A. H., Wong, K. C. and Datta, S. K. (1986) Dynamic stress intensity factors for buried planar and nonplanar cracks. *International Journal of Solids and Structures* **22,** 845–857.

Stone, S. F., Ghosh, M. L. and Mal, A. K. (1980) Diffraction of antiplane shear waves by an edge crack. *Journal of Applied Mechanics* **47,** 359–362.